

RESEARCH

Open Access



# Oncogenic RIT1 mutations confer ferroptosis vulnerability in lung adenocarcinoma

Ruilan Ma<sup>1†</sup>, Dian Yang<sup>2†</sup>, Peng Wang<sup>2</sup>, Ziyi Zhang<sup>2</sup>, Xuehong Zhang<sup>2</sup>, Jialiang Song<sup>2</sup>, Han Liu<sup>2</sup>, Shuyan Liu<sup>2</sup>, Yingqiu Zhang<sup>2\*</sup> and Lijuan Zou<sup>1\*</sup>

## Abstract

Members from the RAS GTPase superfamily have been closely implicated in the tumorigenesis of various human cancers. Recent sequencing analysis of lung adenocarcinoma has revealed the prevalence of alterations in the *RIT1* gene that is a close *RAS* paralog. However, relative to *RAS* subfamily members *KRAS*, *NRAS*, and *HRAS*, our characterization of *RIT1* oncogenic properties remains incomplete. Therefore, further investigation on *RIT1* will facilitate future development of targeted therapies. Our bioinformatic analysis revealed that *RIT1* alterations in lung cancer predicted poor survivals but differed from its *RAS* paralogs by showing largely amplification and mutation. Through biochemical characterization of *RIT1* hotspot mutations, we propose that *RIT1* alterations were associated with increased protein abundance that promoted cell growth. Transcriptomic profiling indicated that oncogenic *RIT1* mutant expression influenced common tumorigenic *RAS*/MAPK, PI3K/AKT, and E2F1 pathways, in addition to altered *NFE2L2* target expression. Importantly, *RIT1* mutants markedly sensitized cells to ferroptosis induction, and *RIT1* knockdown suppressed ferroptotic cell death. Lung adenocarcinoma NCI-H2110 cells containing endogenous *RIT1* M90I mutation were susceptible to ferroptosis induction both in vitro and in vivo within xenograft models. Hence, our study unravels a novel aspect of *RIT1* mutations in lung cancer and suggests ferroptosis induction as a potential therapeutic strategy to treat lung cancer patients carrying *RIT1* mutations.

**Keywords** Lung adenocarcinoma, RAS family, RIT1, GTPase, Ferroptosis, Oncogenic mutation, NRF2

## Background

Lung cancer remains as a leading threat to human health by ranking the top deadly malignancy with an estimated annual incidence of over 2.2 million worldwide [1]. Non-small cell lung cancer (NSCLC) is the principal histological subtype of lung cancer comprising about 85%

of all cases. Major advances in the treatment of clinical NSCLC patients have been achieved by molecular characterizations of the genetic alterations harbored in lung cancer cells [2]. Large scale cancer genomic studies have revealed a number of oncogenic mutations affecting multiple genes that drive NSCLC tumorigenesis. Among these, genetic alterations occurring in *TP53*, *EGFR* and *RAS* family member genes have been found to be highly prevalent in NSCLC [3]. Extensive investigation on the pathological functions and pharmacological intervention of oncogenic epidermal growth factor receptor (EGFR) and *RAS* family proteins has led to the successful development of targeted therapies against these oncoproteins that have considerably prolonged NSCLC patient survivals [2]. Therefore, the ongoing characterization of

<sup>†</sup>Ruilan Ma and Dian Yang contributed equally to this work.

\*Correspondence:

Yingqiu Zhang  
zhangyingqiu.no.1@163.com  
Lijuan Zou  
zouljjuan1963@sina.com

<sup>1</sup>Department of Radiation Oncology, Second Affiliated Hospital, Dalian Medical University, Dalian, China

<sup>2</sup>The Institute of Cancer Stem Cell, Dalian Medical University, Dalian, China



additional oncogenic mutations in alternative therapeutic candidates will likely expedite the development of novel therapeutic strategies to expand the arsenal in the battle against NSCLC.

RAS family proteins are a group of guanosine triphosphate hydrolases (GTPases) that act as molecular switches through alternating forms of GTP binding and hydrolysis to function in many aspects of cellular processes [4]. KRAS, NRAS and HRAS are major members of the RAS subfamily, and have been closely implicated in the tumorigenesis of many kinds of cancer [5]. In lung adenocarcinoma, oncogenic mutations have been detected in KRAS, NRAS and HRAS proteins, with the mutation frequency of *KRAS* gene estimated to be over 30% and thus considered as one of the most frequently mutated genes [6]. Interestingly, recent cancer sequencing analyses revealed that the *RIT1* gene encoding a closely RAS-related GTPase called Ras-like without CAAX 1 (RIT1) was also mutated in NSCLC samples at a frequency (~2%) higher than those for NRAS and HRAS [7]. However, relative to our understanding of KRAS, NRAS and HRAS proteins, the functional characterization of RIT1 wild-type and oncogenic mutants still need to be further elucidated [8].

Ferroptosis is a recently discovered modality of regulated cell death, which emerged from the screening and identification of inhibitors targeting oncogenic RAS-containing cells [9]. Ensuing investigation has confirmed the close association of ferroptosis with tumorigenesis and efficacy in cancer treatment, and hence ferroptosis induction is deemed as a promising therapeutic approach to target multiple cancers including NSCLC [10, 11]. In the present study, we focused on three frequently detected mutants of RIT1 (A77S, F82L and M90I) and confirmed their pro-cancerous activities through phenotypic and sequencing analyses. Our observations suggest that the oncogenic features of mutated RIT1 likely depend on their elevated expression incurred by increased protein stability. On the contrary, the oncogenic mutations in RIT1 protein nevertheless conferred cells a vulnerability to ferroptosis induction, which was observed both *in vitro* and *in vivo*. Our findings thus provide novel insights into the features of oncogenic RIT1 mutants and provide basis for designing therapeutic approaches to target NSCLC containing RIT1 mutations through ferroptosis induction.

## Materials and methods

### Cell culture

NSCLC cell lines A549, H1975, NCI-H2110 and human bronchial epithelial HBE135-E6E7 cells were obtained from the American Type Culture Collection (ATCC) and grown in RPMI-1640 media (Gibco) supplemented with 10% FBS (Gibco) and 1% penicillin/streptomycin

(Thermo Fisher). HEK293T and HeLa cells were generously provided by Prof. Haixin Lei (Dalian Medical University) and were cultured in DMEM (Dulbecco's Modified Eagle's Medium) media (Gibco) supplemented with FBS and antibiotics. All cells were maintained in a 37 °C humidified incubator (Thermo Fisher, 3111) containing CO<sub>2</sub> at 5%.

### Antibodies and reagents

Rabbit anti-RIT1 (ab53720) and rabbit anti-Ki-67 antibodies were purchased from Abcam. Mouse anti- $\alpha$ -Tubulin antibody was purchased from Sigma. Mouse anti-COX2 antibody was purchased from Proteintech (Wuhan, China). Goat anti-mouse and anti-rabbit secondary antibodies (680–800 nm infrared-labeled) were obtained from LICOR. Cycloheximide and DCFH-DA were purchased from Dalian Meilun Biotechnology Co., Ltd. RSL3, IKE (imidazole ketone erastin) and ferrostatin-1 were purchased from MedChemExpress (MCE). BODIPY 581/591 C11 was purchased from Thermo Fisher. Propidium iodide and other general chemicals were obtained from Sigma.

### Generation of stable cell lines

A549 and H1975 cells with stable knockdown of RIT1 were established as previously described [12]. In brief, HEK293T cells were transfected with pLKO.1 plasmids (control and RIT1 shRNA) together with psPAX2 and pMD2.G packaging vectors according to manufacturer's instructions (Sigma). Lentiviruses were harvested after 48 h, which were incubated with A549 and H1975 cells. Positive cells were selected with puromycin treatment and RIT1 knockdown was validated by Western blotting. To generate HBE135-E6E7 cells stably expressing RIT1 wide-type or mutants (A77S, F82L and M90I), wide-type and mutant RIT1 were subcloned into the pCDH vector, which was then used together with psPAX2 and pMD2.G plasmids to co-transfect HEK293T cells using Lipofectamine™ 3000 transfection reagent (Invitrogen) for lentivirus packaging. HBE135-E6E7 cells were infected with lentiviruses and subjected to puromycin selection (2  $\mu$ g/ml).

### Colony formation assay

A549, H1975, and HBE135-E6E7 cells were seeded into six-well plates at a density of 1,000 cells/well. Cells were maintained in the incubator with media replenished every other day. After seven days, cells were gently washed with PBS before fixation using methanol. Subsequently, cells were washed several times with PBS and stained with 0.1% crystal violet for 15 min. The numbers and sizes of cell colonies were quantified using the ImageJ software.

### Measurement of ferroptotic cell death

A549 and HBE135-E6E7 cells were used for evaluation of ferroptosis induction as previously described [13]. For HBE135-E6E7 stable cells,  $2 \times 10^5$  cells were seeded into each well of 6-well plates. After 24-hour incubation at 37 °C, cells were treated with RSL3 (10  $\mu$ M) or RSL3 in combination with ferrostatin-1 (1  $\mu$ M), with DMSO used as a vehicle control. Eight hours post treatment, cells were incubated with propidium iodide (PI). For A549 stable cell lines,  $1 \times 10^5$  cells were seeded into each well of 6-well plates. After 24-hour incubation at 37 °C, cells were treated with RSL3 (20  $\mu$ M) or RSL3 in combination with ferrostatin-1 (2  $\mu$ M), and DMSO was used as vehicle control. Four hours post treatment, cells were stained with PI. Five random views from 10X objective fields were used for image capture and quantification.

### GFP fluorescence microscopy

Cultured HeLa cells were transfected with plasmids expressing GFP-tagged RIT1 constructs using the Polyplus transfection reagent (jetPRIME) and fluorescence staining was performed as previously described [14]. Briefly, 24 h after transfection, cells were washed with PBS and fixed in 4% (w/v) paraformaldehyde for 15 min. Coverslips were then PBS washed, and mounted onto slides in Mowiol containing DAPI. Samples were allowed to air-dry overnight prior to examination under a fluorescence microscope (Olympus BX63, Japan).

### Immunoblot analysis

Immunoblot assays were conducted as described previously [15]. Briefly, cells were lysed using the RIPA buffer before incubated with SDS-PAGE loading buffer at 95 °C for 5 min. Proteins were separated by SDS-PAGE and transferred to nitrocellulose membranes (Millipore). Membranes were blocked with 4% skimmed milk in PBS for 1 h at room temperature. The membranes were then incubated with primary antibodies overnight at 4 °C and secondary antibodies for 1 h at room temperature. Blots were visualized by LICOR Odyssey system. Relative protein levels were calculated using the Image Studio software.

### Transcriptomic profiling

HBE135-E6E7 cells stably transfected with control, wild-type, RIT1 mutants (A77S, F82L and M90I) constructs were harvested with TRIzol reagent (Thermo Fisher). Total RNA was extracted and processed for cDNA library generation as described previously [16]. Paired-end sequencing was conducted using an Illumina NovaSeq 6000 platform. Raw data were first processed to acquire clean reads that were aligned to reference genome using hisat2 version 2.0.5. Gene expression was quantified using featureCounts version 1.5.0-p3, with fragments per

kilo-base of exon per million fragments mapped (FPKM) values obtained. Differentially-expressed genes between groups were evaluated with edgeR version 3.22.5. Enrichment analysis was performed with clusterProfiler version 3.8.1 and GSEA version 3.0.

### Flow cytometry

NCI-H2110 cells were seeded into 6-well plates and treated with DMSO or 5  $\mu$ M of RSL3 for 6 h on the next day. For ROS detection and lipid peroxidation assay, cells were washed using PBS prior to incubation with 10  $\mu$ M of DCFH-DA or 5  $\mu$ M of BODIPY 581/591 C11, respectively, for 30 min at 37 °C. Subsequently, cells were trypsinized and resuspended in ice-cold PBS in the dark, and immediately fluorescence signals were collected using the Accuri C6 Plus flow cytometer (BD Biosciences). Acquired data were analyzed using the FlowJo software (version 10).

### Xenograft mouse model

Mouse experiment procedures were assessed and approved by the Institutional Animal Care and Use Committee at Dalian Medical University. Female nude mice (BALB/c background, 4–6 weeks) were obtained from Vital River Co. Ltd. (Beijing, China) and kept in SPF animal center. NCI-H2110 cells (1.5 million) were subcutaneously implanted into nude mice. When sizes of xenografts reached  $\sim 50 \text{ mm}^3$ , mice were randomly divided into two groups (5 mice/group), which were administered with IKE (40 mg/kg) or DMSO as vehicle control by intraperitoneal injection every day. After 28 days post inoculation, xenografts were dissected and weighed. Tumor volume was calculated using the formula:  $(\text{length}) \times (\text{width})^2 \times 0.5$ .

### Immunohistochemistry

Xenograft samples were subjected to formalin fixation immediately after resection. Tissues were then embedded in paraffin and cut to 5  $\mu$ m thick slices. Prepared tissue sections were deparaffinized with xylene and rehydrated with graded alcohol. Following incubation with blocking solution using the IHC assay kit (ZSGB-Bio, Beijing, China), tissue sections were incubated with anti-Ki-67 and anti-COX-2 antibodies overnight at 4 °C. Next day, sections were stained using the IHC assay kit according to the manufacturer's instructions. Images were taken by a phase contrast microscope (Leica) and analyzed by Image-Pro Plus software (version 6.0).

### Statistical analysis

Each experiment was repeated at least three times. All data were demonstrated as the mean  $\pm$  S.E. (standard errors). The statistical analyses were completed using Prism GraphPad, using Student's t test (for two group

comparison), one-way or two-way ANOVA (for multiple groups) analysis. The KM plot showing overall survival was generated using R and difference between groups was assessed by log rank test. In general, a p value smaller than 0.05 was considered statistically significant.

**Results**

**RIT1 alterations in NSCLC are associated with increased RIT1 protein expression**

Taking advantage of the cancer genomics data integrated by the cBioPortal platform (cbioportal.org), we analyzed the alterations of *KRAS*, *HRAS*, *NRAS*, and *RIT1* paralog genes occurring in NSCLC samples [17–19]. As shown in Fig. 1A, the 4 closely related genes showed different

alteration features across multiple cohorts of NSCLC patients. Considering the types of alteration, the *KRAS* gene was primarily mutated in NSCLC tissues, while changes in *NRAS* and *HRAS* genes were similar by showing largely both mutation and deletion. In addition, the frequency of *KRAS* gene alteration was often observed to be above 20%, which was noticeably higher than those of *NRAS* and *HRAS* that were merely around 2% (Fig. 1A). Unlike the *RAS* paralogs, the alterations of *RIT1* gene in NSCLC were predominantly amplification in addition to a fraction being mutation, and the frequency of *RIT1* alteration could reach above 5% depending on different datasets (Fig. 1A). Since RIT1 alterations appeared to be more prominent in lung adenocarcinoma, we decided to

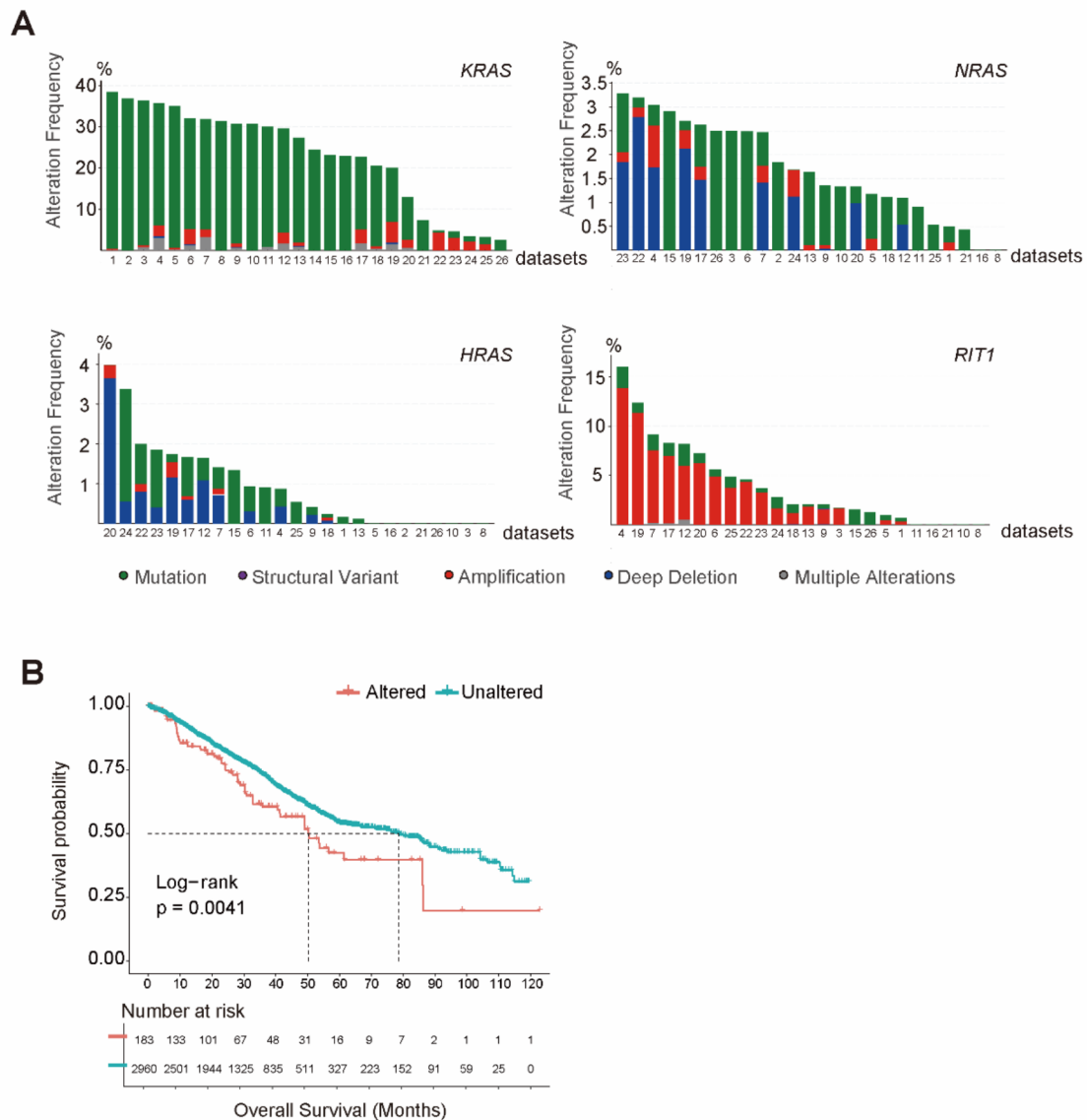


**Fig. 1** Lung cancer-associated *RIT1* alterations predict worse prognosis and differ from those observed in *KRAS*, *HRAS*, and *NRAS*. **(A)** Frequencies of various genomic alterations of *KRAS*, *HRAS*, *NRAS*, and *RIT1* in NSCLC patients were analyzed with the cBioPortal platform (<https://www.cbioportal.org/>). **(B)** Kaplan–Meier curve showing overall survival stratified by altered *RIT1* vs. unaltered *RIT1*. Statistical difference was examined using the log-rank test



M90I). Using a GFP tagging approach, we first examined the intracellular distribution of wild-type and mutated RIT1 proteins. As shown in Fig. 2C, different versions of RIT1 exhibited similar localization by showing both nuclear and cytoplasmic distribution. Importantly, all versions of RIT1 exhibited evident membrane localization when transiently expressed in HeLa cells, suggesting that these oncogenic mutations likely not affecting RIT1 distribution. Subsequently, we established stable RIT1 expression cell lines (wild-type and mutants) using the bronchus epithelial HBE135-E6E7 cells. Results from Western blot analysis indicate that the expression levels of three mutated forms of RIT1 were significantly higher than wild-type albeit with the same expression system and cell background (Fig. 2D). Therefore, we carried out cycloheximide chase experiments to compare the turnover rates of mutated RIT1 with that of wild-type. As shown in Fig. 2E, the oncogenic RIT1 mutants were considerably more stable than wild-type version, providing the explanation of their increased protein abundance in the same cellular system. Our results are thereby consistent with previous study reporting reduced association of oncogenic RIT1 mutants with its cognate E3 ligase LZTR1 to avoid ubiquitylation-mediated degradation leading to increased RIT1 protein levels [22]. Collectively, our bioinformatic analysis and preliminary biochemical characterization suggest that cancer-associated alterations in RIT1 gene (amplification and mutation) led to increased RIT1 protein expression to promote tumorigenesis of NSCLC.

#### **RIT1 knockdown deters lung adenocarcinoma cell growth but mutant expression promotes proliferation**

It has been proposed that RIT1 functions to activate the canonical PI3K/AKT and MAPK pathways that are pivotal oncogenic signaling cascade in many cancer types, and hence RIT1 mutations are considered mutually exclusive with those acquired by other key signaling modules in the pathway such as RAS members. It is noteworthy that previous studies mainly focused on the mutation alterations of *RIT1* gene in the investigation. Since our bioinformatic analysis unveiled the relatively high frequency of amplification changes in *RIT1* gene, we reexamined the correlations of *RIT1* alterations with those of its *RAS* paralogs in lung adenocarcinoma using cBioPortal integrated analysis. As shown in Fig. 3A, mutual exclusivity analysis revealed that KRAS, HRAS, and NRAS showed mutual exclusive tendencies against each other, but RIT1 exhibited co-occurrence tendencies with all three RAS members. Based on this observation, we decided to assess the influence of RIT1 knockdown on cell growth of lung adenocarcinoma harboring activating mutations on the RAS/MAPK pathway. As such, we depleted RIT1 expression using two separate shRNAs

in A549 and H1975 cells that contained KRAS G12S and EGFR T790M mutations, separately. Using these stable RIT1 knockdown cells, we performed colony formation assays and found that the depletion of RIT1 evidently decreased cell propagation (Fig. 3B and C). Therefore, our findings suggest that RIT1 function is not dispensable in lung adenocarcinoma cells containing activating mutations in the RAS-MAPK pathway.

We then examined the effects of RIT1 mutant expression using abovementioned HBE135-E6E7 cells stably expressing RIT1 wild-type or the A77S, F82L and M90I mutants. As shown in Fig. 3D, results from colony formation assays show that the expression of A77S, F82L and M90I versions of RIT1 noticeably enhanced cell proliferation, while wild-type RIT1 did not elicit a significant impact. To gain more insights into the underlying mechanisms of the pro-tumor effects of RIT1 mutations, we conducted transcriptomic profiling analysis of HBE135-E6E7 cells stably transfected with control, RIT1 wild-type, or the A77S, F82L and M90I mutant constructs. As demonstrated in Fig. 4A, principal component analysis shows that cells transfected with wild-type and mutant constructs are separated from the control group, while the 3 mutants can be clustered together. Furthermore, we generated a heatmap to illustrate differentially-expressed genes (DEGs) among 5 groups, and also observed that the A77S, F82L and M90I oncogenic mutants demonstrated similar alterations comparing to the vector control and wild-type (Fig. 4B). We next performed GO (Gene Ontology) and KEGG (Kyoto Encyclopedia of Genes and Genomes) enrichment analyses of DEGs between wild-type and mutated RIT1 groups. As shown in Fig. 4C and D, top listed pathways enriched by GO and KEGG analysis include the MAPK/ERK cascade, PI3K/AKT pathway, RAS signaling that are well-established vital tumorigenic signaling cascades. As expected, our observations are in accordance with previous results from transcriptomic and proteomic characterizations of oncogenic RIT1 mutations [23].

In order to further explore features associated with oncogenic RIT1 mutations, we conducted oncogenic signature enrichment analysis with DEGs incurred by RIT1 mutant expression as compared to wild-type version. Interestingly, in addition to KRAS and E2F1 gene sets that are closely implicated in tumor progression, the *NFE2L2* gene set also appeared in the top list (Fig. 4E). This gene set contains over 400 factors involved in cellular redox sensing and regulation, which are primarily downstream targets of the NFE2 transcription factor but some candidates can also be regulated by other transcription factors. Therefore, our sequencing analysis suggests that, in addition to activate canonical tumorigenic signaling pathways, oncogenic RIT1 mutant expression

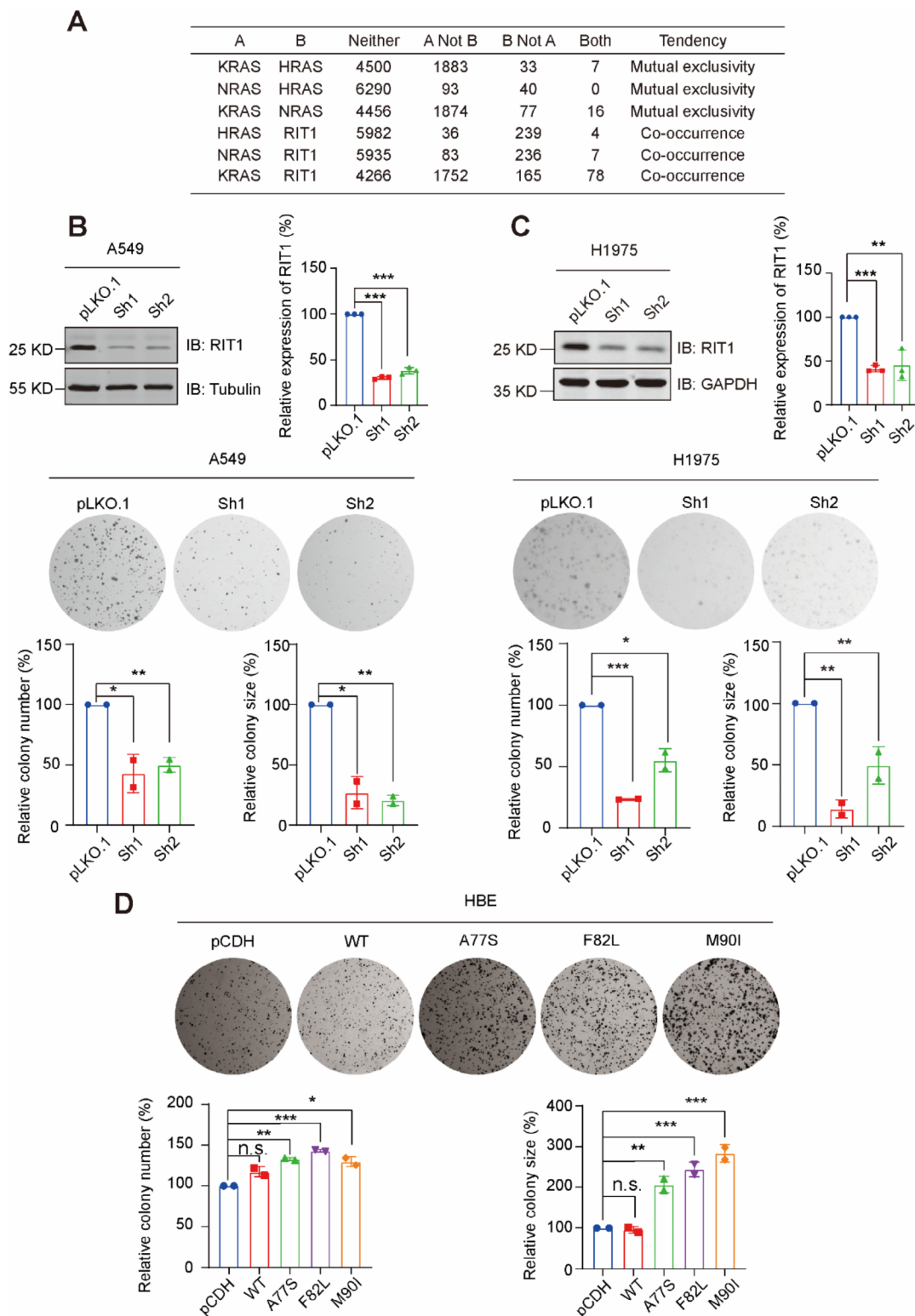


**Fig. 3** Depletion of RIT1 inhibits proliferation of lung adenocarcinoma cells and RIT1 A77, F82 and M90 mutations promote cell growth. **(A)** Correlation analysis of RIT1 alterations with those of its RAS paralogs in lung adenocarcinoma with cBioPortal platform (<https://www.cbioportal.org/>). **(B and C)** The efficiency of RIT1 knockdown in A549 and H1975 cells was validated by immunoblotting. Tubulin or GAPDH was used as protein loading control. Below images and column charts show representative colony formation assays and quantification of colony number and size. **(D)** Colony formation assays performed using HBE135-E6E7 stable cell lines with WT or mutated RIT1 overexpression as indicated. Quantification was conducted using ImageJ software. Data were presented as mean  $\pm$  s.e.m. \* $P < 0.05$ , \*\* $P < 0.01$ , \*\*\* $P < 0.001$ . n.s., not significant

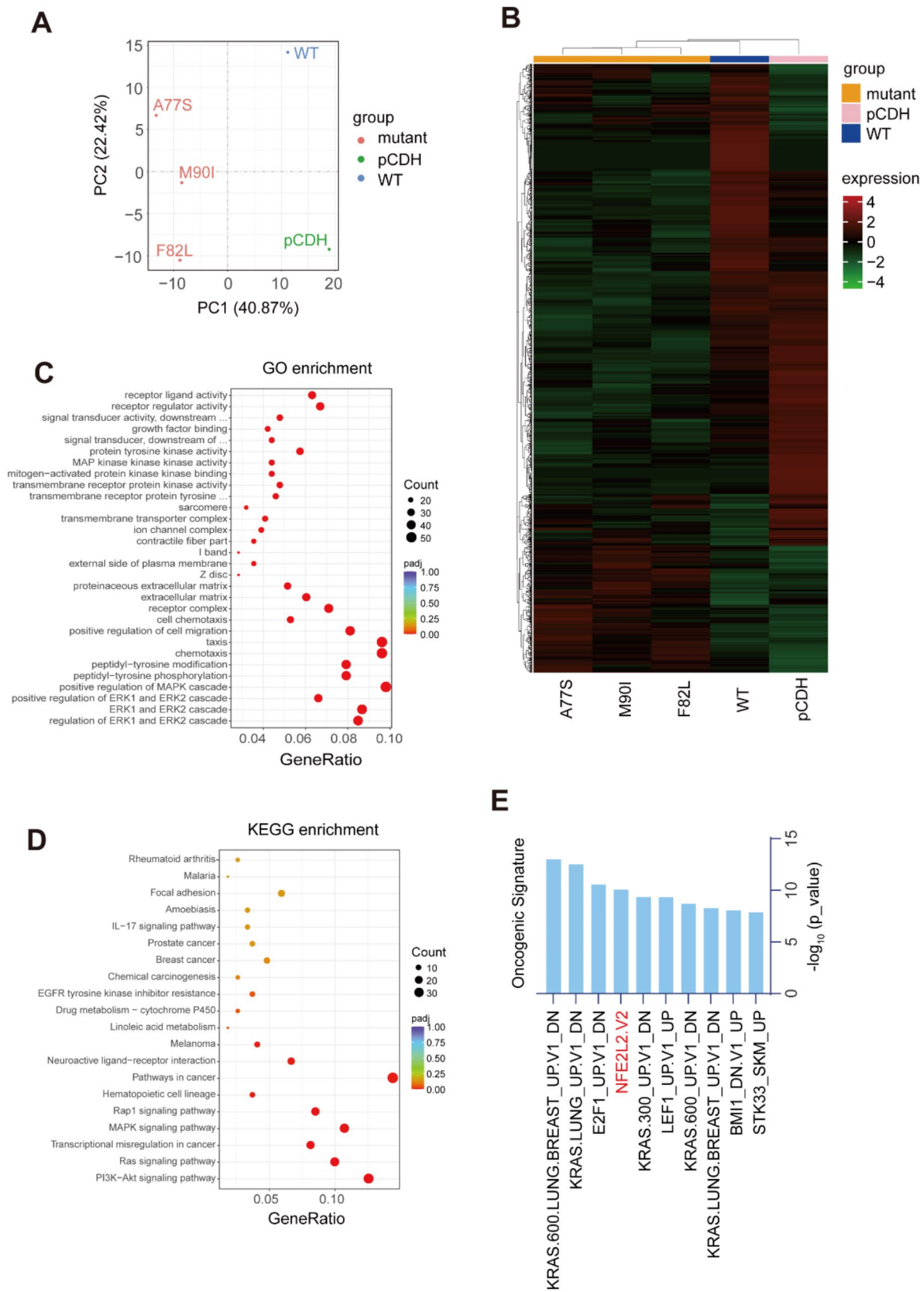


**Fig. 4** Transcriptomic profiling of cells expressing RIT1 wild-type and oncogenic mutations. **(A)** Principal component (PC) analysis of RNA-seq data for control vector (pCDH), WT (wild-type) and mutant groups. **(B)** Heat map illustrating differentially-expressed genes (DEGs) among 5 groups as indicated. **(C** and **D)** GO (Gene Ontology) and KEGG (Kyoto Encyclopedia of Genes and Genomes) enrichment analysis of DEGs between WT RIT1 and mutant groups. **(E)** Oncogenic signature enrichment analysis of DEGs between WT RIT1 and mutant groups

also leads to changes in the expression of cellular redox regulators.

### RIT1 expression regulates sensitivity to cellular ferroptosis induction

Next, we performed GSEA analysis to further examine the influence of mutant RIT1 expression on NRF2 downstream target expression. As shown in Fig. 5A and

B, results from GSEA analysis and volcano plot of DEG analysis indicated that mutant RIT1 expression led to a bi-directional influence on NRF2 target expression, with more candidates showing a downregulatory effect. Considering the essential roles of NRF2 targets in cellular redox homeostasis and ferroptosis prevention, we wondered whether oncogenic RIT1 expression would affect the sensitivity of cells to ferroptosis induction [24, 25]. To

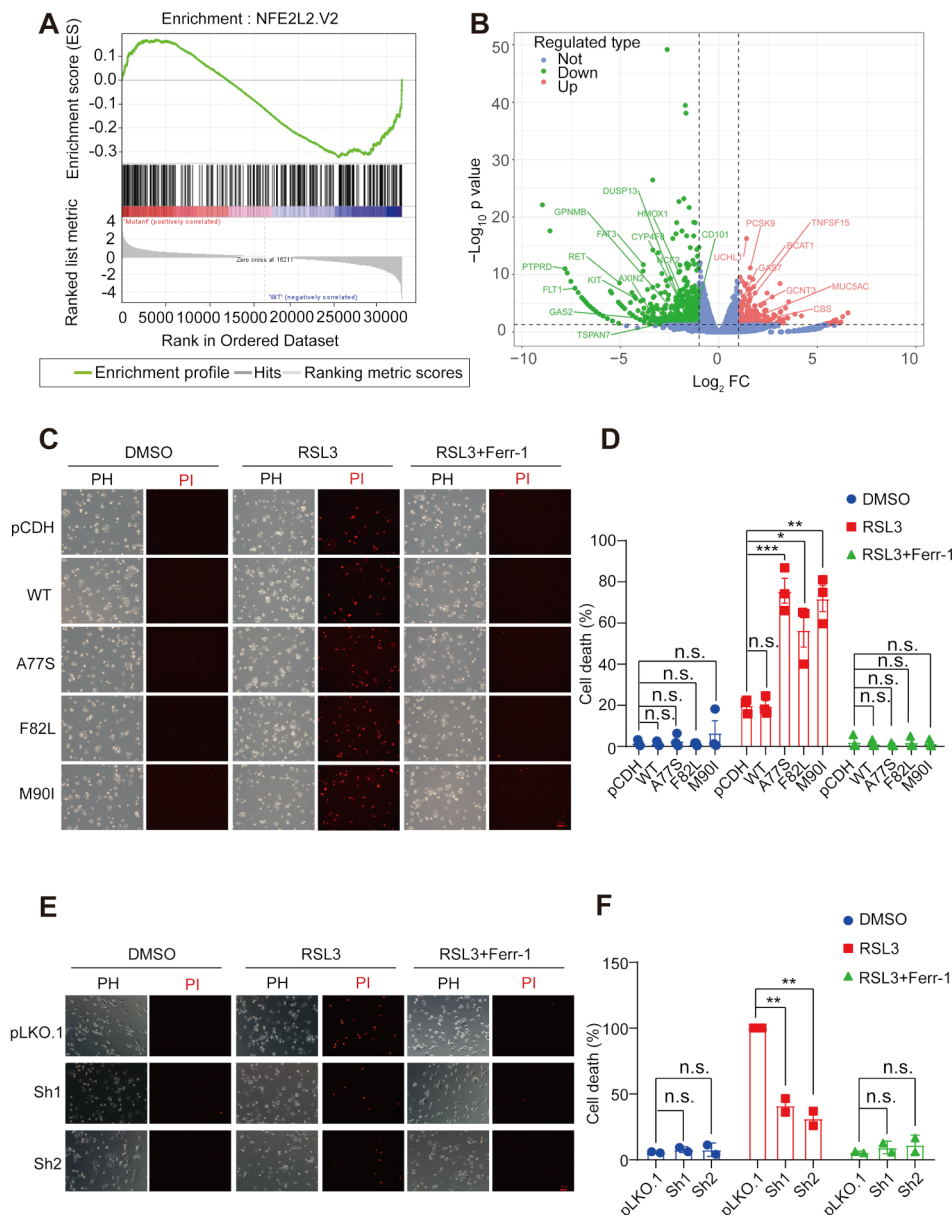


**Fig. 5** Oncogenic RIT1 mutations sensitize cells to ferroptosis induction and RIT1 depletion suppresses ferroptosis. **(A)** RNA-seq data were subjected to GSEA analysis with *NFE2L2* gene set. **(B)** Volcano plot demonstrating significantly changed NRF2 target genes from RNA-seq data. **(C and D)** Representative images **(C)** and the quantification of cell death **(D)** of the propidium iodide (PI) stained HBE135-E6E7 stable cell lines with indicated treatment under phase contrast (PH) or fluorescence microscope. Cells were treated with RSL3 (10  $\mu$ M) in the presence or absence of ferrostatin-1 (1  $\mu$ M) for 8 h. **(E and F)** Representative images **(E)** and the quantification of cell death **(F)** of A549 derived stable cells with indicated treatment under phase contrast (PH) or fluorescence microscope. Cells were treated with RSL3 (20  $\mu$ M) in the presence or absence of ferrostatin-1 (2  $\mu$ M) for 4 h. Data were presented as mean  $\pm$  s.e.m. \* $P$  < 0.05, \*\* $P$  < 0.01, \*\*\* $P$  < 0.001. n.s., not significant

this end, we treated HBE135-E6E7 cells stably expressing RIT1 wild-type or the A77S, F82L and M90I mutants with the GPX4 inhibitor RSL3 that is a potent ferroptosis inducer [26, 27]. As illustrated in Fig. 5C and D, oncogenic RIT1 mutations rendered HBE135-E6E7 cells more susceptible to RSL3-induced ferroptosis, which was efficiently blocked by the ferroptosis inhibitor ferrostatin-1. Furthermore, we triggered ferroptosis in A549 cells with or without stable RIT1 depletion. As shown in Fig. 5E and F, shRNA-mediated RIT1 knockdown significantly reduced the percentages of cells undergoing ferroptosis in A549 cells. Collectively, our ferroptosis induction assays using cells with RIT1 knockdown or mutant over-expression suggest that RIT1 protein levels were correlated with cellular sensitivity to ferroptosis.

#### **Oncogenic RIT1-containing lung cancer xenografts are susceptible to ferroptosis induction**

Despite of the relative low frequency of *RIT1* mutation, lung adenocarcinoma NCI-H2110 cell line has been found to contain the M90I mutation in *RIT1* gene, providing a suitable model to characterize endogenous oncogenic RIT1 [28]. As shown in Fig. 6A, NCI-H2110 was susceptible to ferroptosis induction by RSL3, which was efficiently reversed by the ferroptosis inhibitor ferrostatin-1. Furthermore, RSL3 treatment also led to significant increases of both cellular ROS (reactive oxygen species) and lipid ROS levels in NCI-H2110 cells, indicative of evident increase in lipid peroxidation (Fig. 6B and C). To investigate the contribution of oncogenic M90I mutant in ferroptotic cell death, we knocked down endogenous RIT1 expression using two separate shRNAs. As shown in Fig. 6D, both shRNAs effectively depleted RIT1 protein levels, with sh2 showing a stronger effect. Accordingly, we compared ferroptosis occurrence in pLKO control and sh2 stable NCI-H2110 cells following RSL3 treatment. Consistently, RIT1 knockdown rendered NCI-H2110 sh2 cells reduced susceptibility to RSL3-induced ferroptosis that was accompanied with decreased ROS levels, indicating that RIT1 was indeed involved in the regulation of sensitivity to ferroptotic cell death in NCI-H2110 cells (Fig. 6E-G). After confirming ferroptosis induction with NCI-H2110 cells in vitro, we turned to investigate the sensitivity of NCI-H2110 xenografts towards ferroptosis inducer IKE that was preferred for in vivo use with nude mouse models [27, 29]. Mice with subcutaneously implanted NCI-H2110 xenografts were randomized to receive vehicle or IKE treatment, and xenograft tumors were measured to calculate sizes over the course of experiment. As shown in Fig. 7A and B, IKE treatment efficiently hindered NCI-H2110 xenograft growth. Subsequent immunohistochemical analysis of resected tissues showed that IKE treatment resulted in reduced expression of the proliferation marker Ki-67 but

led to increased levels of the ferroptosis marker COX-2 (Fig. 7C and D). Taken together, results from our in vivo animal model experiments are in accordance with our in vitro analysis and collectively suggest that RIT1 mutant expression effectively potentiated ferroptosis induction.

#### **Discussion**

Molecular characterizations of human cancers have dramatically deepened our understanding of various driver mutations in malignancies and provided guidelines how to precisely target distinct oncoproteins in the clinical treatment of human cancers. Fundamental research and clinical investigation have led to the successful development of targeted therapies against oncogenic EGFR, KRAS (G12C), ALK fusion proteins to treat NSCLC patients. Interestingly, accumulating genomic data from lung cancer tissue sequencing have revealed the RAS paralog RIT1 as a frequently altered driver in lung adenocarcinoma [7, 30]. Ensuing investigation has confirmed the oncogenic properties of mutated RIT1 and explored its downstream signaling output as well as potential targets for synthetic lethality treatment [23, 31]. Besides lung adenocarcinoma, RIT1 alterations have been implicated in the tumorigenesis of other cancer types including endometrial cancer and glioblastoma, in addition to the major type of RASopathy called Noonan syndrome [32–35].

Although RIT1 shares a high degree of similarity with the 3 RAS paralogs, its oncogenic mutations frequently occur in or close to the switch-II (residues 78–93) region, differing from most hotspot mutations observed in RAS proteins [8]. Such unique pattern of RIT1 mutations in lung cancer likely suggests alternative regulatory mechanisms compared to the other RAS proteins. Indeed, our bioinformatic analysis of RIT1 alterations in NSCLC revealed that amplification of *RIT1* was noticeably more dominant relative to mutation and deletion, which was opposite to alterations characterized in RAS proteins that were primarily mutation and deletion. Furthermore, our biochemical characterizations of RIT1 mutants confirmed that these mutations led to increased RIT1 abundance by inhibiting its degradation. Taken together, our findings suggest that RIT1 alterations in NSCLC are associated with elevated RIT1 protein expression, in stark contrast with major RAS oncogenic mutations that predominantly interfere with nucleotide binding and hydrolysis [36].

Oncogenic RAS mutants have been recognized as notoriously difficult to inhibit and for a certain period of time considered as “undruggable”, thus posing great challenges to the clinical treatment of patients carrying these mutations. Fortunately, recent development of sotorasib and adagrasib that target KRAS G12C mutation through covalent binding has shown successful clinical efficacy

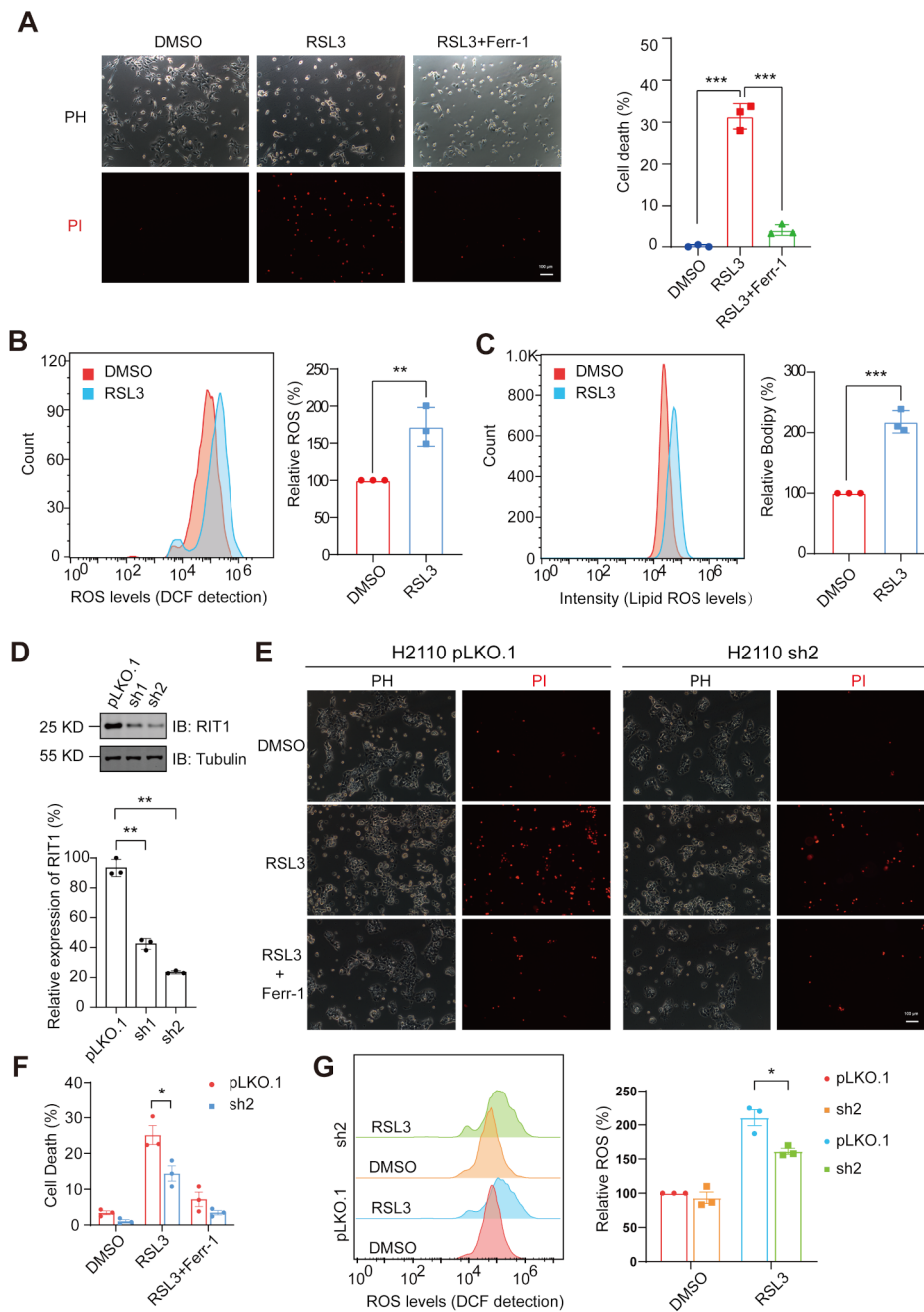


**Fig. 6** NCI-H2110 cells with endogenous M90I mutation in *RIT1* are susceptible to ferroptosis induction. **(A)** Representative images and quantification of cell death in NCI-H2110 cells with indicated treatment under phase contrast (PH) or fluorescence microscope. Cells were treated with RSL3 (5  $\mu$ M) in the presence or absence of ferrostatin-1 (1  $\mu$ M) for 24 h. **(B and C)** Flow cytometric analysis of intracellular ROS **(B)** and lipid ROS levels **(C)** in NCI-H2110 cells with or without RSL3 using indicated probes. **(D)** Western blotting analysis of NCI-H2110 cells stably transfected with control vector (pLKO.1) and shRNAs targeting *RIT1* (sh1 and sh2). Tubulin was probed as loading control. Column chart shows quantification of relative *RIT1* expression. **(E)** Representative images and **(F)** quantification of cell death in NCI-H2110 stable cells (pLKO.1 and sh2) with indicated treatment under phase contrast (PH) or fluorescence microscope. Cells were treated with RSL3 (5  $\mu$ M) in the presence or absence of ferrostatin-1 (1  $\mu$ M) for 12 h. **(G)** Flow cytometric analysis of intracellular ROS levels in NCI-H2110 stable cells (pLKO.1 and sh2) with or without RSL3 treatment. Data were presented as mean  $\pm$  s.e.m. \* $P$  < 0.05, \*\* $P$  < 0.01, \*\*\* $P$  < 0.001

and been approved by authorities [37]. However, targeted therapies are still unavailable regarding oncogenic *RIT1* and other *RAS* mutants, although extensive investigation is currently being performed trying to resolve such

unmet needs. In this study, we focused on oncogenic *RIT1* mutations in lung adenocarcinoma and confirmed their stimulating effects on cell propagation. Through transcriptomic analysis of cells expressing mutant versus

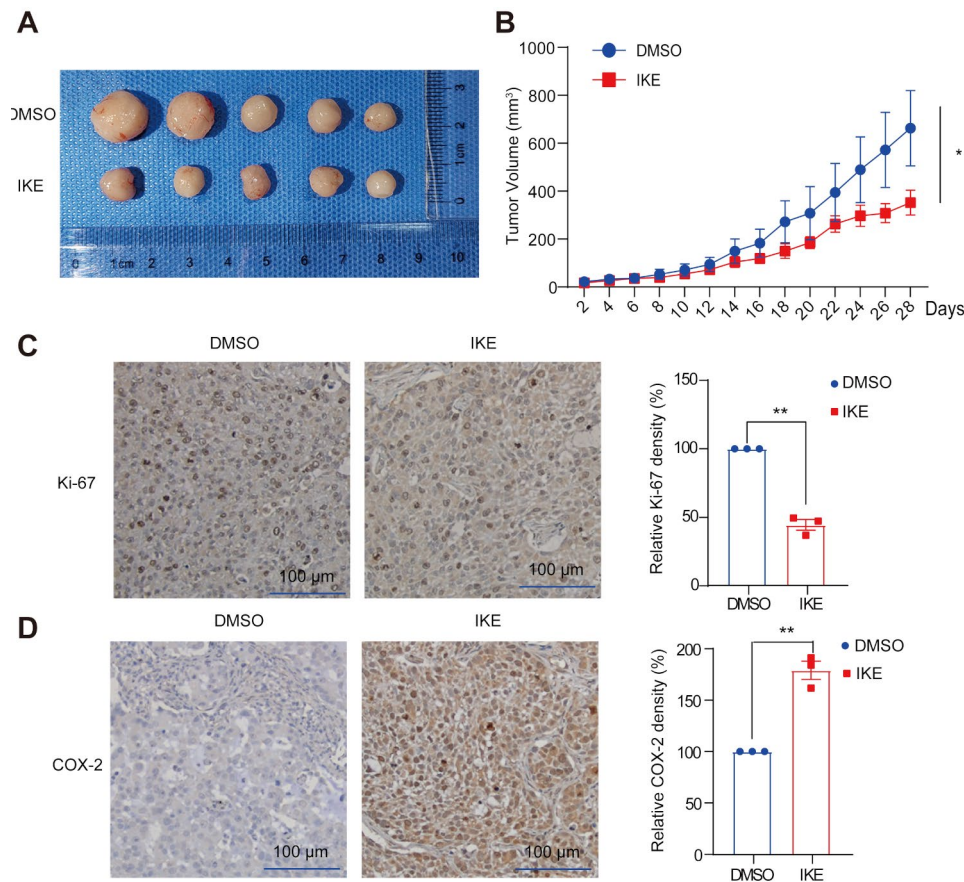


**Fig. 7** NCI-H2110 xenografts are sensitive to in vivo ferroptosis induction. **(A)** Image of resected NCI-H2110 xenograft tumors from nude mice with or without IKE treatment at day 28. **(B)** Growth curves showing volumes of the NCI-H2110 xenografts with or without IKE treatment at indicated times. **(C)** and **(D)** Representative immunohistochemistry images and corresponding quantification of Ki-67 and COX-2 staining with NCI-H2110 xenograft samples. Data were presented as mean  $\pm$  s.e.m. \* $P < 0.05$ , \*\* $P < 0.01$

wild-type RIT1, in addition to the upregulation of common tumorigenic RAS/MAPK and PI3K/AKT pathways, we observed that RIT1 mutant expression was also associated with altered expression in downstream targets of the redox master regulator NRF2. Concomitant with growth stimulation, oncogenic RIT1 mutations also conferred cells with increased sensitivities to ferroptosis induction by RSL3. Importantly, sensitivity to ferroptosis induction was also observed in NCI-H2110 lung adenocarcinoma cells that contain RIT1 M90I mutant using in vivo xenograft mouse model analysis. Since a growing number of NRF2 downstream targets are shown to regulate cellular ferroptosis occurrence, further investigation on RIT1 is warranted to dissect its key downstream signaling molecules implicated in this important type of regulated cell death.

## Conclusion

In a summary, our findings collectively suggest that RIT1 alterations in lung adenocarcinoma are frequently manifested by increased protein expression. However,

oncogenic RIT1 mutations confer increased ferroptosis sensitivity thus presenting a vulnerability that can be exploited in future investigation to develop therapeutic strategies against oncogenic RIT1.

## Abbreviations

RIT1	Ras like without CAAX1
RAS	Rat sarcoma
GTPase	GTP hydrolases
KRAS	Kirsten rat sarcoma viral oncogene
NRAS	NRAS proto-oncogene, GTPase
HRAS	HRas Proto-Oncogene, GTPase
MAPK	Mitogen-activated protein kinase
PI3K	Phosphoinositide 3-kinase
AKT	Protein kinase B
E2F1	E2F transcription factor 1
NFE2L2/NRF2	Nuclear factor erythroid 2-related factor 2
NSCLC	Non-small cell lung cancer
TP53	Tumor protein p53
EGFR	Epidermal growth factor receptor
Met	Methionine
Ala	Alanine
Phe	Phenylalanine
LZTR1	Leucine Zipper Like Post Translational Regulator 1
DCFH-DA	H2DCFDA
shRNA	Short hairpin RNA

PBS	Phosphate Buffer Saline
DMSO	Dimethyl sulfoxide
FPKM	Fragments per kilo-base of exon per million fragments mapped
CHX	Cycloheximide
IHC	Immunohistochemistry
Ki-67	Proliferation marker protein Ki-67
COX-2	Cytochrome c oxidase subunit 2
DEGs	Differentially-expressed genes
GO	Gene Ontology
KEGG	Kyoto Encyclopedia of Genes and Genomes
GAPDH	Glyceraldehyde-3-phosphate dehydrogenase
PC	Principal component
GPX4	Glutathione Peroxidase 4
PI	Propidium iodide
PH	Phase contrast
ROS	Reactive oxygen species
IKE	Imidazole ketone erastin

### Acknowledgements

The authors are grateful to Prof. Haixin Lei for generously providing cell lines. We also want to thank Mr. Bo Shi for bioinformatic assistance.

### Author contributions

YZ and LZ designed the project. YZ supervised the study. RM, DY, PW, ZZ, XZ, and JS performed experiments and analyzed data. RM, DY, PW, HL, SL and YZ interpreted the data. YZ and RM wrote the manuscript. All authors reviewed the manuscript.

### Funding

This study was supported by the General Project of the Educational Department of Liaoning Province (LJKMZ20221275 to YZ).

### Data availability

Data is provided within the manuscript or supplementary information files.

### Declarations

#### Ethics approval and consent to participate

Animal experiments were obtained approval from the Institutional Animal Care and Use Committee at Dalian Medical University.

#### Consent for publication

The publication has been approved by all co-authors.

#### Competing interests

The authors declare no competing interests.

Received: 28 July 2024 / Accepted: 28 January 2025

Published online: 07 February 2025

### References

- Sung H, Ferlay J, Siegel RL, Laversanne M, Soerjomataram I, Jemal A, Bray F. Global Cancer statistics 2020: GLOBOCAN estimates of incidence and Mortality Worldwide for 36 cancers in 185 countries. *Cancer J Clin.* 2021;71(3):209–49.
- Sharma SV, Bell DW, Settleman J, Haber DA. Epidermal growth factor receptor mutations in lung cancer. *Nat Rev Cancer.* 2007;7(3):169–81.
- Kandoth C, McLellan MD, Vandin F, Ye K, Niu B, Lu C, Xie M, Zhang Q, McMichael JF, Wyczalkowski MA, et al. Mutational landscape and significance across 12 major cancer types. *Nature.* 2013;502(7471):333–9.
- Bernal Astrain G, Nikolova M, Smith MJ. Functional diversity in the RAS sub-family of small GTPases. *Biochem Soc Trans.* 2022;50(2):921–33.
- Omerovic J, Laude AJ, Prior IA. Ras proteins: paradigms for compartmentalised and isoform-specific signalling. *Cell Mol Life Sci.* 2007;64(19–20):2575–89.
- Prior IA, Hood FE, Hartley JL. The frequency of ras mutations in Cancer. *Cancer Res.* 2020;80(14):2969–74.
- Cancer Genome Atlas Research N. Comprehensive molecular profiling of lung adenocarcinoma. *Nature.* 2014;511(7511):543–50.
- Van R, Cuevas-Navarro A, Castel P, McCormick F. The molecular functions of RIT1 and its contribution to human disease. *Biochem J.* 2020;477(15):2755–70.
- Dixon SJ, Lemberg KM, Lamprecht MR, Skouta R, Zaitsev EM, Gleason CE, Patel DN, Bauer AJ, Cantley AM, Yang WS, et al. Ferroptosis: an iron-dependent form of nonapoptotic cell death. *Cell.* 2012;149(5):1060–72.
- Chen X, Kang R, Kroemer G, Tang D. Broadening horizons: the role of ferroptosis in cancer. *Nat Reviews Clin Oncol.* 2021;18(5):280–96.
- Jiang X, Stockwell BR, Conrad M. Ferroptosis: mechanisms, biology and role in disease. *Nat Rev Mol Cell Biol.* 2021;22(4):266–82.
- Sun Q, Zhang J, Li X, Yang G, Cheng S, Guo D, Zhang Q, Sun F, Zhao F, Yang D, et al. The ubiquitin-specific protease 8 antagonizes melatonin-induced endocytic degradation of MT(1) receptor to promote lung adenocarcinoma growth. *J Adv Res.* 2022;41:1–12.
- Wang S, Wang T, Zhang X, Cheng S, Chen C, Yang G, Wang F, Wang R, Zhang Q, Yang D, et al. The deubiquitylating enzyme USP35 restricts regulated cell death to promote survival of renal clear cell carcinoma. *Cell Death Differ.* 2023;30(7):1757–70.
- Wang T, Zhang J, Wang S, Sun X, Wang D, Gao Y, Zhang Y, Xu L, Wu Y, Wu Y, et al. The exon 19-deleted EGFR undergoes ubiquitylation-mediated endocytic degradation via dynamin activity-dependent and -independent mechanisms. *Cell Communication Signaling: CCS.* 2018;16(1):40.
- Zhang J, Liu S, Li Q, Shi Y, Wu Y, Liu F, Wang S, Zaky MY, Yousuf W, Sun Q, et al. The deubiquitylase USP2 maintains ErbB2 abundance via counteracting endocytic degradation and represents a therapeutic target in ErbB2-positive breast cancer. *Cell Death Differ.* 2020;27(9):2710–25.
- Liu S, Wang T, Shi Y, Bai L, Wang S, Guo D, Zhang Y, Qi Y, Chen C, Zhang J, et al. USP42 drives nuclear speckle mRNA splicing via directing dynamic phase separation to promote tumorigenesis. *Cell Death Differ.* 2021;28(8):2482–98.
- Cerami E, Gao J, Dogrusoz U, Gross BE, Sumer SO, Aksoy BA, Jacobsen A, Byrne CJ, Heuer ML, Larsson E, et al. The cBio cancer genomics portal: an open platform for exploring multidimensional cancer genomics data. *Cancer Discov.* 2012;2(5):401–4.
- Gao J, Aksoy BA, Dogrusoz U, Dresdner G, Gross B, Sumer SO, Sun Y, Jacobsen A, Sinha R, Larsson E, et al. Integrative analysis of complex cancer genomics and clinical profiles using the cBioPortal. *Sci Signal.* 2013;6(269):p11.
- de Bruijn I, Kundra R, Mastrogiacomo B, Tran TN, Sikina L, Mazor T, Li X, Ochoa A, Zhao G, Lai B, et al. Analysis and visualization of longitudinal genomic and clinical data from the AACR Project GENIE Biopharma Collaborative in cBioPortal. *Cancer Res.* 2023;83(23):3861–7.
- Jumper J, Evans R, Pritzel A, Green T, Figurnov M, Ronneberger O, Tunyasuvunakool K, Bates R, Zidek A, Potapenko A, et al. Highly accurate protein structure prediction with AlphaFold. *Nature.* 2021;596(7873):583–9.
- Varadi M, Bertoni D, Magana P, Paramval U, Pidruchna I, Radhakrishnan M, Tsenkov M, Nair S, Mirdita M, Yeo J, et al. AlphaFold protein structure database in 2024: providing structure coverage for over 214 million protein sequences. *Nucleic Acids Res.* 2024;52(D1):D368–75.
- Castel P, Cheng A, Cuevas-Navarro A, Everman DB, Papageorge AG, Simanshu DK, Tankka A, Galeas J, Urisman A, McCormick F. RIT1 oncoproteins escape LZTR1-mediated proteolysis. *Science.* 2019;363(6432):1226–30.
- Lo A, Holmes K, Kamlapurkar S, Mundt F, Moorthi S, Fung I, Fereshtian S, Watson J, Carr SA, Mertins P, et al. Multiomic characterization of oncogenic signaling mediated by wild-type and mutant RIT1. *Sci Signal.* 2021;14(711):eabc4520.
- Anandhan A, Dodson M, Schmidlin CJ, Liu P, Zhang DD. Breakdown of an Ironclad Defense System: the critical role of NRF2 in mediating ferroptosis. *Cell Chem Biology.* 2020;27(4):436–47.
- Yan R, Lin B, Jin W, Tang L, Hu S, Cai R. NRF2, a superstar of Ferroptosis. *Antioxidants* 2023, 12(9).
- Yang WS, Stockwell BR. Synthetic lethal screening identifies compounds activating iron-dependent, nonapoptotic cell death in oncogenic-RAS-harboring cancer cells. *Chem Biol.* 2008;15(3):234–45.
- Stockwell BR, Jiang X. The Chemistry and Biology of Ferroptosis. *Cell Chem Biology.* 2020;27(4):365–75.
- Berger AH, Brooks AN, Wu X, Shrestha Y, Chouinard C, Piccioni F, Bagul M, Kamburov A, Imielinski M, Hogstrom L, et al. High-throughput phenotyping of Lung Cancer somatic mutations. *Cancer Cell.* 2016;30(2):214–28.
- Larraufie MH, Yang WS, Jiang E, Thomas AG, Slusher BS, Stockwell BR. Incorporation of metabolically stable ketones into a small molecule probe to increase potency and water solubility. *Bioorg Med Chem Lett.* 2015;25(21):4787–92.
- Berger AH, Imielinski M, Duke F, Wala J, Kaplan N, Shi GX, Andres DA, Meyerson M. Oncogenic RIT1 mutations in lung adenocarcinoma. *Oncogene.* 2014;33(35):4418–23.

31. Vichas A, Riley AK, Nkinsi NT, Kamlapurkar S, Parrish PCR, Lo A, Duke F, Chen J, Fung I, Watson J, et al. Integrative oncogene-dependency mapping identifies RIT1 vulnerabilities and synergies in lung cancer. *Nat Commun.* 2021;12(1):4789.
32. Xu F, Sun S, Yan S, Guo H, Dai M, Teng Y. Elevated expression of RIT1 correlates with poor prognosis in endometrial cancer. *Int J Clin Exp Pathol.* 2015;8(9):10315–24.
33. Khalil A, Nemer G. The potential oncogenic role of the RAS-like GTP-binding gene RIT1 in glioblastoma. *Cancer Biomark A.* 2020;29(4):509–19.
34. Aoki Y, Niihori T, Banjo T, Okamoto N, Mizuno S, Kurosawa K, Ogata T, Takada F, Yano M, Ando T, et al. Gain-of-function mutations in RIT1 cause Noonan syndrome, a RAS/MAPK pathway syndrome. *Am J Hum Genet.* 2013;93(1):173–80.
35. Chen PC, Yin J, Yu HW, Yuan T, Fernandez M, Yung CK, Trinh QM, Peltekova VD, Reid JG, Tworog-Dube E, et al. Next-generation sequencing identifies rare variants associated with Noonan syndrome. *Proc Natl Acad Sci USA.* 2014;111(31):11473–8.
36. Burge RA, Hobbs GA. Not all RAS mutations are equal: a detailed review of the functional diversity of RAS hot spot mutations. *Adv Cancer Res.* 2022;153:29–61.
37. Singhal A, Li BT, O'Reilly EM. Targeting KRAS in cancer. *Nat Med.* 2024;30(4):969–83.

### **Publisher's note**

Springer Nature remains neutral with regard to jurisdictional claims in published maps and institutional affiliations.